atmosphere

Article

Indoor Radon Monitoring and Associated Diffuse Radon Emissions in the Flanks of Mt. Etna (Italy)

Nunzia Voltattorni [1], Salvatore Giammanco [2], Gianfranco Galli [1], Andrea Gasparini [1] and Marco Neri [2,*]

[1] Istituto Nazionale di Geofisica e Vulcanologia-Sezione Roma 1, 00143 Roma, Italy; nunzia.voltattorni@ingv.it (N.V.); gianfranco.galli@ingv.it (G.G.); andrea.gasparini@ingv.it (A.G.)
[2] Istituto Nazionale di Geofisica e Vulcanologia-Osservatorio Etneo, Sezione di Catania, 95125 Catania, Italy; salvatore.giammanco@ingv.it
* Correspondence: marco.neri@ingv.it

Abstract: Between October 2021 and July 2024, radon measurements in air and soil were carried out in the South and East flanks of Etna volcano to check the possible correlation between radon emissions and active faults/eruptive fissures and to obtain preliminary data on any negative impacts on human health. Fifteen continuous indoor radon monitors were installed in homes, some of which are inhabited by patients suffering from Multiple Sclerosis and Amyotrophic Lateral Sclerosis. In all sites, the limit of 300 Bq/m^3 indicated by the Euratom Directive 2013/59 was exceeded, even if slightly and for short periods. The highest values were recorded closest to active fault zones and during winters. Furthermore, 27 discrete indoor radon measurements were carried out using a passive method by means of activated charcoal canisters that were exposed for 48 h. Most of the values (>70%) were <100 Bq/m^3; six canisters gave values >100 Bq/m^3 and one >200 Bq/m^3. Measurements of radon in soils were carried out using a Durridge RAD7 in the gardens of the homes in which the indoor radon measurements were made. The background radon values in soils were <5000 Bq/m^3; the highest values (12,500 Bq/m^3) were measured near the Aci Catena fault. The role of Etna's faults in draining the deeper radon towards the surface and, therefore, into nearby homes is evident, with a consequent increase in the health risk caused by indoor radon pollution.

Keywords: radon; Etna; faults; eruptive fissures; human health

check for updates

Citation: Voltattorni, N.; Giammanco, S.; Galli, G.; Gasparini, A.; Neri, M. Indoor Radon Monitoring and Associated Diffuse Radon Emissions in the Flanks of Mt. Etna (Italy). *Atmosphere* **2024**, *15*, 1359. https://doi.org/10.3390/atmos15111359

Academic Editor: Boris Igor Palella

Received: 14 September 2024
Revised: 7 November 2024
Accepted: 9 November 2024
Published: 12 November 2024

1. Introduction

Radon (Rn) is a natural radioactive gas, whose distribution on Earth is widespread because of the relatively high concentration of its parent nuclides in the rocks making the crust of our planet. As a result of its physical and chemical properties, it is used in Geosciences as a tool for studying both the dynamics of magma and magmatic gases inside active volcanoes [1–9] and those of active faulting in tectonic [10–17] and volcano-tectonic [18–22] regions.

However, this gas can also produce highly detrimental effects on human health because of its radioactivity [23–26]. In particular, long-term exposure to high levels of radon can cause a higher incidence of lung cancer [27–30] or of lymphocytic leukemia [31]. The EU Council Directive 2013/59/EURATOM fixes the maximum level of Rn indoors to 300 Bq/m^3, which is also the highest annual average Rn concentration not to be exceeded, according to World Health Organization [32], in case the limit of 100 Bq/m^3 was reached under the predominant country-specific conditions.

Volcanic areas are known for the higher emission of Rn from the local magmatic rocks, because these are richer in U and U-bearing minerals [15,33,34]. Furthermore, active volcanoes are also intersected by faults that, in general, act as pathways for the transport and release of magmatic/volcanic gases, and, hence, Rn, to the surface. For these reasons, Rn is widely used as a tracer of volcanic and/or tectonic processes near the surface [33–38].

Mt. Etna, one of the most active volcanoes in the world (Figure 1), is extensively studied and monitored by the Istituto Nazionale di Geofisica e Vulcanologia (henceforth, INGV) for the diffuse emissions of Rn gas from the soil in relation with the magma transfer and stress accumulation within its edifice [39–41].

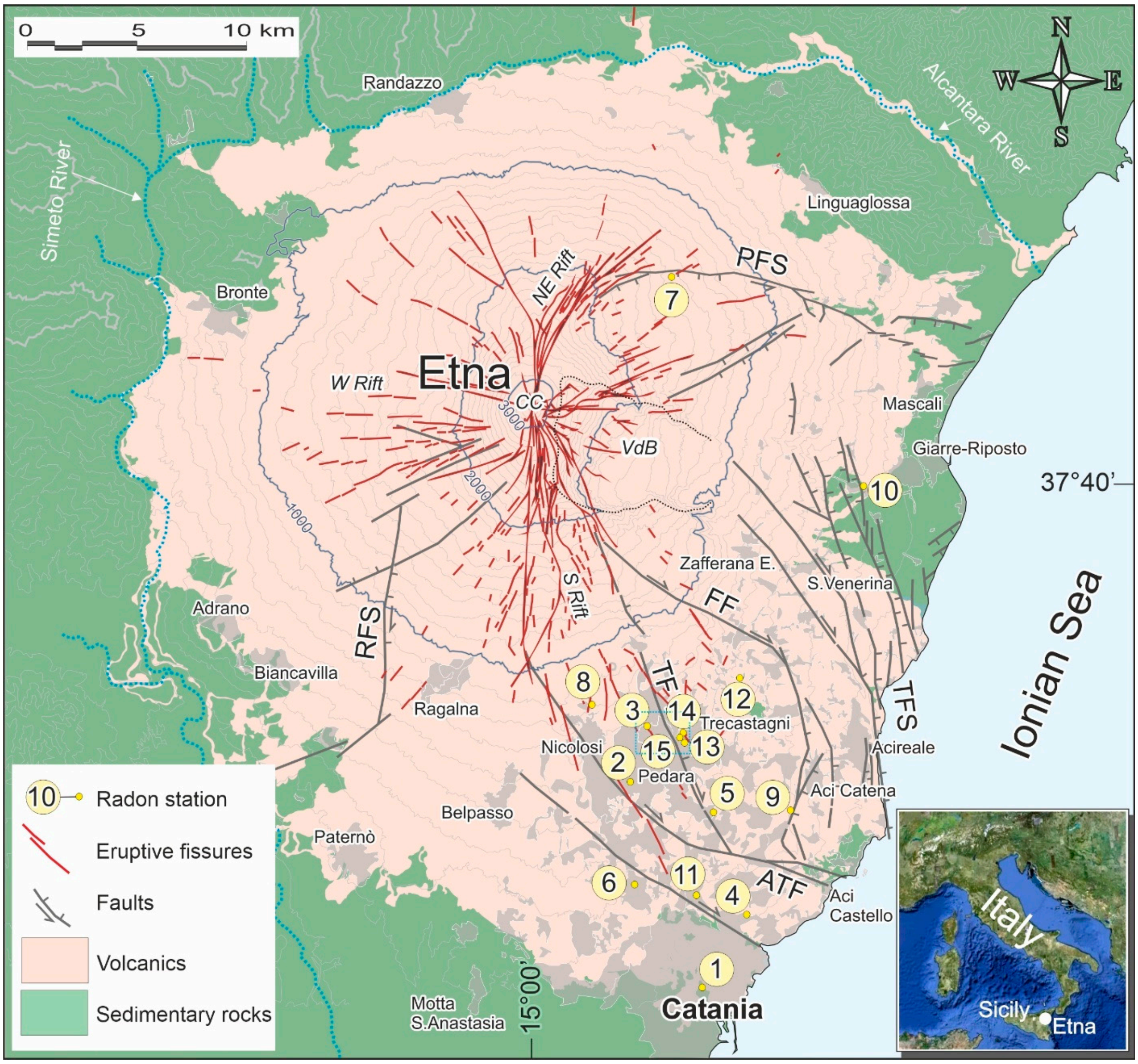

Figure 1. The simplified geostructural map of Mt. Etna depicts the principal fault lines crossing the volcano and the locations of indoor radon measurements, numbered from 1 to 15. The urbanized regions are represented by light gray tones; contour lines are expressed in meters above sea level. PFS, Pernicana fault system; RFS, Ragalna fault system; TFS, Timpe fault system; FF, Fiandaca fault; TF, Trecastagni fault; ATF, Aci Trezza fault. VdB, Valle del Bove; CC, Central Craters. The light blue rectangle with a dotted outline indicates the area of Figure 4 and Figure 5.

Recent studies on the spatial distribution of in-soil Rn concentrations showed a clear correlation between higher Rn emissions and fault planes [33,36,37,39]. This led to the discovery of several hidden or buried faults that are actively degassing, but were not known before [16,22,39]. Many of the faults on Mt. Etna cross urban areas, thus highlighting the potential health risk of indoor Rn accumulation in nearby houses [40,41]. Figure 2 illustrates the release of radon gas in a volcanic setting and its subsequent transfer into the atmosphere and into human dwellings. Recent surveys on indoor Rn in some buildings on Mt. Etna showed that houses within a few hundred meters from a fault had average indoor Rn levels well above the threshold of 300 Bq/m^3, with Rn concentrations following an exponential increase on moving closer to the fault [40,41]. Furthermore, indoor Rn levels were, in general, much higher during the winter and very low during the summer [42], clearly because of the more efficient ventilation of the houses during the hot Sicilian months when windows are often kept open during most of the day.

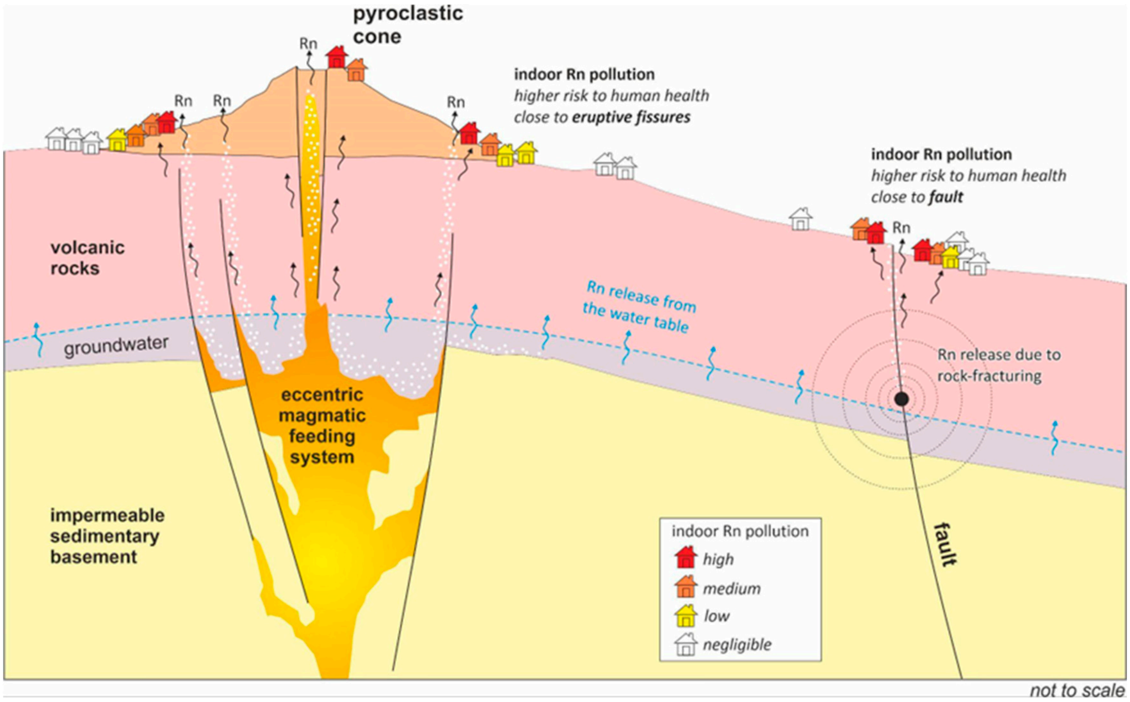

Figure 2. Schematic model of radon transport and release at the surface through faults or volcano-tectonic structures at Mt. Etna, with a qualitative scale of the level of impact of indoor radon accumulation as a function of the distance of the houses from the natural pathways (see blue and black arrows) of radon emission.

This study was aimed at investigating in more detail the ways Rn escapes from the ground and accumulates in homes at Mt. Etna. Many of the monitored dwellings were selected among those with people suffering from diseases that are suspected to be triggered either by the exposure to trace elements in volcanic emissions or by the exposure to radiations (i.e., Multiple Sclerosis, Amyotrophic Lateral Sclerosis, and Primary Brain Tumors). For the first time on this volcano, in-soil Rn measurements were coupled with indoor Rn detection and monitoring and air Rn monitoring over a time span of some years in a wide area of the south flank of Mt. Etna.

2. Materials and Methods

Between October 2021 and December 2023, several detailed field surveys were carried out in the S and E flanks of Etna volcano (Sicily, Southern Italy), which included both indoor and in-soil radon measurements (Figure 1). Detailed soil radon-gas surveys were carried out during the dry seasons, which, in Sicily, essentially corresponds to the summer months. They consisted of 153 measurements of radon and thoron activity, among which 139 were carried out within an area including Pedara and Trecastagni villages and 14 in different yards of private dwellings (at Aci Catena, Mascalucia, Linguaglossa, Giarre, San Gregorio, San Giovanni La Punta, and San Pietro Clarenza villages) where indoor radon canisters were exposed.

2.1. Soil Radon-Gas and Thoron Sampling

Soil radon-gas (^{222}Rn) and thoron (^{220}Rn) concentrations were measured with a portable certified alpha spectrometer, model RAD7 (DURRIDGE Company, Inc., Billerica, MA, USA) (Figure 3a). Once the radon and thoron particles enter the detection chamber, their decay produces positively charged ^{218}Po and ^{216}Po ions, respectively, which are subsequently collected on the solid-state detector via an electric high-voltage field. We set our instrument in sniff mode, which is suitable for fast measurements. In this way, only alpha decays from ^{218}Po and ^{216}Po are counted. Therefore, temporary radon and thoron concentrations were recorded in 5 min intervals over a 15 min period (imposed by the time necessary for ^{218}Po and ^{222}Rn nuclei to reach radioactive equilibrium, which is approximately 5 times the half-life of ^{218}Po; note that 2 min intervals over a 6 min period would be enough to reach radioactive equilibrium between ^{216}Po and ^{220}Rn nuclei). The gas was pumped from a steel probe inserted at a depth of at least 0.50 m into the soil. An inlet filter and a desiccant trap (drierite) were used to protect the detector from dust and soil moisture (relatively, humidity of inlet gas should be maintained below 10%). The instrumental detection limit is +500 Bq/m^3. Both the calibration and the linearity of the employed RAD7 instruments used were previously verified by using a radon chamber [43].

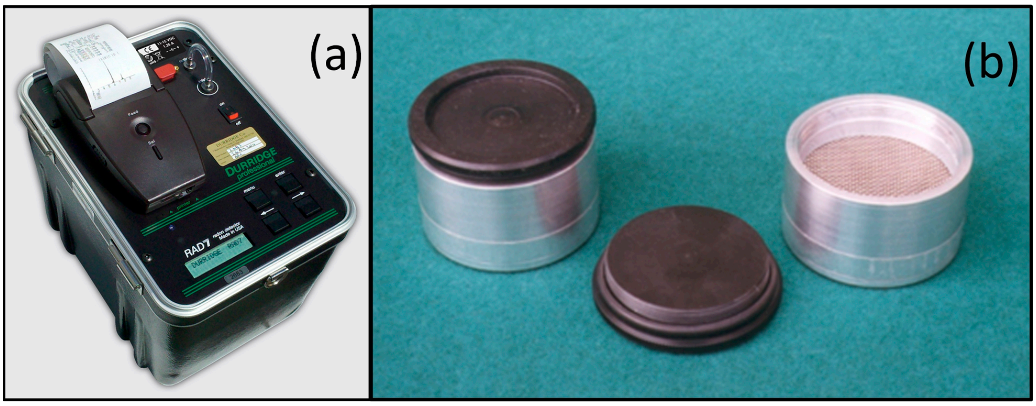

Figure 3. (**a**) Portable alpha spectrometer used for in-soil radon measurements; and (**b**) activated charcoal canisters (ACC) used for discrete measurements of indoor radon concentration.

All field analytical data were subjected to graphical processing, in order to obtain the optimal spatial definition both of geochemical lineaments and of anomalies. Descriptive statistics, including mean, median, variance, standard deviation, skewness, and kurtosis, were employed to describe the data from a basic statistical point of view. A variogram-based interpolation for surface analysis of data was utilized to perform a geostatistical treatment of gas distribution, thereby refining the assessment of the spatial continuity of gas concentration anomalies and achieving useful parameters for the construction of a contour-line map.

2.2. Indoor Radon Sampling

We carried out 27 spot measurements of indoor radon in private homes using activated charcoal canisters (ACC—Figure 3b). The ACC passive method is useful in order to perform simultaneous measurements in the same site. The canisters can be reused after being regenerated through heating, at 125 °C for at least 10 h. We calibrated each ACC in a specific radon chamber. In the chamber, radon with known activity Rn is introduced, and then both the temperature T and the relative humidity RH are varied at defined levels over time. In order to complete the calibration, each ACC is exposed for 48 h. A different calibration factor is obtained for the specific type of ACC and the typical detection limit is 8 Bq/m^3 [44].

In situ, the ACC method entails the placement of a canister on the floor of a room for a period of two days, with windows and doors closed to simulate poor air circulation.

Afterwards, the canisters are removed and the activity of Rn is determined with γ spectrometry using a 3″ × 3″ NaI(Tl) scintillator. The main γ lines investigated (ROIs) are those emitted in β decays of ^{214}Pb and ^{214}Bi. In order to calculate this, the following steps must be undertaken:

(i) Choose an acquisition time (T) to add up the counts in the selected ROIs;
(ii) Measure the background counts (B);
(iii) Measure the gross counts (G) from each exposed collector;
(iv) Measure the counts (S) from a standard collector (same size, material, and amount of activated charcoal) with, dispersed, a known activity (A) of ^{226}Ra in equilibrium with ^{222}Rn;
(v) Calculate a factor (AF), whose formula is derived from the ACC calibration, as a function of the water gain (G) absorbed by the collector;
(vi) Calculate the decay factor (DF) accounting for radon decay from the median exposure time to the median measurement time;
(vii) Apply the following equation [45]:

$$\mathrm{Rn}\ (\mathrm{Bq/m^3}) = [(\mathrm{G} - \mathrm{B})/\mathrm{T}]/[\mathrm{ET} \times \mathrm{AF}(\mathrm{G}, \mathrm{ET}) \times (((\mathrm{S} - \mathrm{B})/\mathrm{T})/\mathrm{A}) \times \mathrm{DF}] \quad (1)$$

Indoor radon levels were continuously monitored over long time periods using portable Rn monitors, mod. AER+ (ALGADE, Bessines-sur-Gartempe, France). This is an active monitor provided with a photodiode that detects the alpha particles emitted by radioactive decay of Rn and converts them into electrical pulses. The detected electrical pulses are thus counted by an electronic board during a pre-set time period (15 min in our cases), at the end of which the built-in electronic board calculates the Rn activity (in Bq/m^3) based on the number of electrical pulses counted, the measurement period, and the calibration coefficients of the device, expressed in Becquerel per cubic meter per count per hour (Bq/m^3/c/h). Each monitor is also able to measure ambient temperature and humidity (averaged over the same time range as the Rn measurements) and all data are stored in a datalogger, to be later downloaded onto a laptop PC at regular intervals. At the end of each time period, Rn, temperature and humidity values measured during that period are also shown on a display. AER+ monitors work with an alkaline 1.5 V battery and are able to store data for about six months before filling their internal memory. Their typical sensitivity is 15–20 (Bq/m^3/c/h) and the measurement uncertainty is $\pm$18 Bq/m^3 over 24 h for a Rn level of 300 Bq/m^3. The measurement range is 0–99 kBq/m^3.

2.3. Radon Continuous Monitoring

A fixed station was installed for continuous monitoring of radon gas both in the soil and in the air.

The station consisted of a PVC pipe, stuck in the ground to a depth of approximately 50 cm, that hosted an AER+ at its bottom. At the top of the pipe, there were two Gore-Tex caps, in order to ensure a radon exhalation similar to that of the surrounding soil. A second AER+ radon monitor was installed near the top of the pipe, 1 m above the ground surface, so that the measured values represented a proxy to the channelized exhalation rate of radon, through the pipe, from the soil surface to the atmosphere near the ground. Both monitors were set to measure every hour and both of them were connected to a router for the transmission of data. The data acquired were sent to an FTP account, from which it could be downloaded remotely. The station was in operation from 26 June 2023 to 30 April 2024, with some gaps in the data due to power failures of the instruments used.

3. Results

3.1. Soil Radon Surveys

The in-soil radon survey started during October 2021, carrying out measurements in gardens of private dwellings where indoor radon measurements were made. After the first results of the latter measurements, the soil radon-gas survey was pointed towards an area between the Pedara and Trecastagni villages where indoor radon monitoring highlighted the highest values (see Section 3.2). In an area of about 6 km^2, 139 radon and thoron measurements were taken. Table 1 shows the statistical results for ^{222}Rn and ^{220}Rn soil gas activity levels. The radon values ranged from 128 to 12,500 Bq/m^3, with the mean, median, and standard deviation of 2065, 1540, and 1980 Bq/m^3, respectively. This indicates that the distribution of this gas was slightly skewed. The thoron values ranged from 50 to 189,000 Bq/m^3. The mean and median values were different, as well as the standard deviation, indicating that the distribution of the values was skewed. In fact, the values of the skewness for both isotopes are markedly positive, thus confirming the multivariate (seemingly log-normal) distribution of the data.

Table 1. Statistical results of ^{222}Rn and ^{220}Rn soil gas levels in Pedara–Trecastagni. All values are in Bq/m^3.

Pedara–Trecastagni Area	^{222}Rn	^{220}Rn
n° of measurements	139	139
Min value	128	50
Max value	12,500	189,000
Mean	2065	11,499
Median	1540	8670
Standard Deviation	1980	17,110
Skewness	2.2	8.4

A valid statistical approach for studying data variability and skewed distributions is the use of normal probability plots (NPPs) that allow the recognition both of high anomalous values (outliers) and of threshold values [46]. This approach highlighted multiple populations (e.g., background or extreme data points being very different from the rest of values) corresponding to natural processes that influence the distribution density. The statistical threshold between normal and anomalous values has been identified at 4750 Bq/m^3 and at 12,900 Bq/m^3 for ^{222}Rn and ^{220}Rn, respectively.

The experimental variograms were elaborated in order to estimate the spatial continuity (in terms of geometry and continuity) of values. Figure 4a shows both the experimental variogram and the fitting model for the spatial ^{222}Rn distribution along the axes of anisotropy (28°) and with an angular tolerance of 18°. The x-axis shows the lag distance (distance between pairs of values at which the variogram is calculated) and the y-axis shows the equation for computing the variogram. The fitting models are a spherical function where sample pairs are autocorrelated up to a distance of approximately 400 m (after which the variogram reaches the asymptotic threshold value of 0.295 γ) and the nugget variance, representing the threshold value, which, in this case, is set at 0.1 γ. The elaborated variogram has been used in the kriging calculation for a better evaluation of the radon concentration contour map (Figure 4b). The maximum anisotropy has an N-S orientation and crosses the Pedara municipality. The distribution of radon anomalies highlights the presence of high permeability pathways (i.e., faults and fractures) along which the short-lived Rn can migrate to reach the surface. Furthermore, the orientation of the N-S anomaly fits well with the trend of the well-known Mt. Troina pyroclastic cone and related eruptive fissures [47].

The ^{220}Rn short half-life (55 s) is sufficiently long-lived to indicate that the primary source (U or Th) of the radon anomaly in the soil is likely to be the presence of mineralization close to the surface. This is because the rapid transport of this gas causes high ^{220}Rn levels. However, when the ^{222}Rn and ^{220}Rn distributions overlap, it is reasonable to infer that the two gases have the same origin and can migrate to the surface because of the presence of discontinuities (faults and fractures). Figure 5a shows the experimental variogram and the relative fitting model that has been used for kriging interpolation. The ^{220}Rn distribution map (Figure 5b) shows the same N-S anisotropy found for ^{222}Rn at the Pedara area.

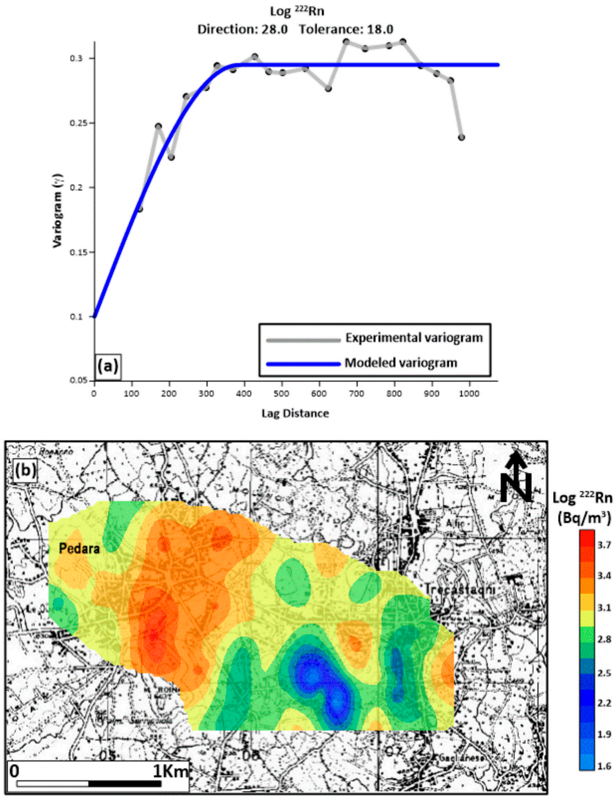

Figure 4. (**a**) Variograms (experimental and modeled) and (**b**) distribution map of ^{222}Rn values measured in soil in the Pedara–Trecastagni area. See text for details.

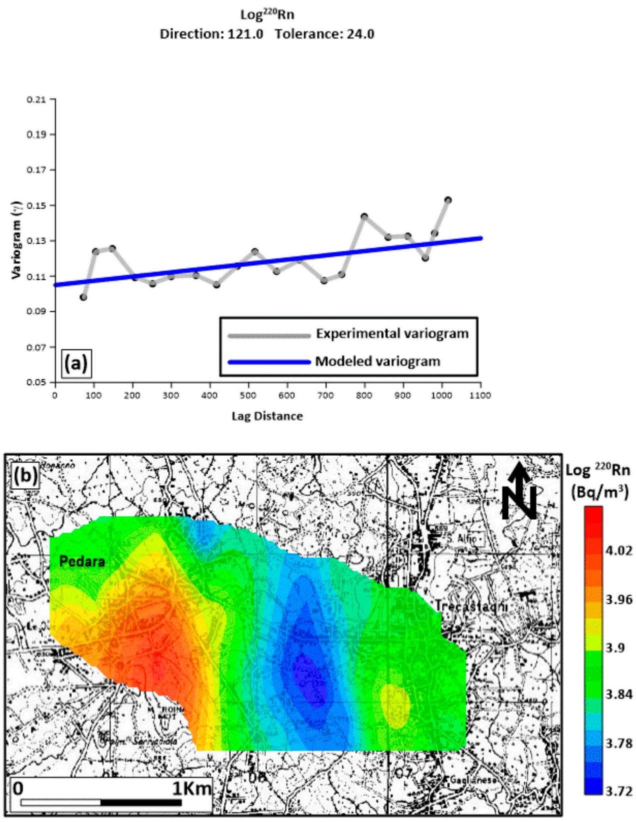

Figure 5. (**a**) Variograms (experimental and modeled) and (**b**) distribution map of ^{220}Rn values measured in soil in the Pedara–Trecastagni area. See text for details.

3.2. Indoor Radon Screening

Twenty-seven charcoal canisters were placed on the floor of 13 private homes where rooms were set up for indoor radon measurements. Six of the selected homes were inhabited by patients suffering from neurodegenerative diseases, others by inhabitants that decided to collaborate voluntarily with data collection. Ideally, canisters should be placed at the lower level of a building, such as cellars (e.g., storerooms) or basements (hobby rooms or workrooms). However, this was not always feasible due to the diversity in the structure of available dwellings. Consequently, canisters were situated in seven cellars, three basements, sixteen ground floors, and one first floor. Table 2 is a summary of the geographical location of the charcoal canisters, their placement in the monitored houses, and also the activity values obtained from the indoor radon measurements carried out in several municipalities in the S and E flanks of Etna volcano. Table 3 shows some statistics on the results of indoor radon measurements, divided by the type of floor in the monitored houses: the values ranged from 8 to 214 Bq/m^3. Both the standard deviation and mean values measured in cellars were similar, thus suggesting a log-normal distribution of data (skewness value = 0.001). The coefficient of variation (CV) shows that data variability is limited for basement values (CV = 0.5), but it is not for ground floor or cellar values (CV = 0.7 and 1.0, respectively).

Table 2. Geographical coordinates (UTM, WGS-84) of the sites where charcoal canisters were placed for indoor radon monitoring, with indication of the type of floor the monitors were placed on and the radon values (in Bq/m^3) obtained from each monitor. 'bdl' is reported for concentrations below the detection limit.

Location Name	Lat.	Long.	Floor	^{222}Rn(Bq/m^3)
Mascalucia	504056	4161322	Ground	106 ± 14
Linguaglossa	505922	4184307	Ground	142 ± 13
			Basement	150 ± 14
Pedara_1	505619	4163974	Ground	65 ± 11
			Cellar	52 ± 10
			Ground	42 ± 10
Pedara_2	505303	4165821	Ground	214 ± 16
			Ground	146 ± 12
San Gregorio	509423	4155231	Ground	47 ± 14
			Cellar	30 ± 18
San Giovanni La Punta	508224	4159485	Ground	114 ± 46
			Cellar	134 ± 46
San Pietro Clarenza	502218	4157219	Basement	60 ± 32
			Ground	57 ± 37
Macchia di Giarre	514547	4174853	Ground	21 ± 39
			Ground	80 ± 48
Sant'Agata Li Battiati	506829	4156130	Ground	20 ± 19
			Ground	29 ± 18
Trecastagni_1	507138	4162644	Cellar	8 ± 36
			Cellar	41 ± 33
			1st	77 ± 34
Trecastagni_2	507086	4163067	Cellar	16 ± 41
			Cellar	bdl
			Basement	66 ± 42
Trecastagni_3	507100	4163233	Ground	37 ± 20
Tarderia	504948	4167787	Ground	bdl
			Ground	bdl

Table 3. Descriptive statistics on the radon values (in Bq/m^3) obtained from the charcoal canisters, divided by the type of floor the monitors were placed on.

	Ground Floor	Basement	Cellar	1st Floor
Number of measures	16	3	7	1
Minimum	20	60	8	77
Maximum	214	150	134	77
Arithmetic Mean	80	92	47	77
Median	61	66	36	n.d.
Standard Deviation	57	50	46	n.d.
IQR	77	n.d.	36	n.d
Lower Quartile	37	n.d.	16	n.d.
Upper Quartile	114	n.d.	52	n.d.
CV	0.7	0.5	1.0	n.d.

Figure 6 shows the data from Table 2 graphically, using box plots. The box plots highlight the variability of the values. Basements have the highest radon values, but they are all below the concentration of 300 Bq/m^3. This is the threshold level of indoor radon exposure allowed by the 2013/59 Euratom Directive.

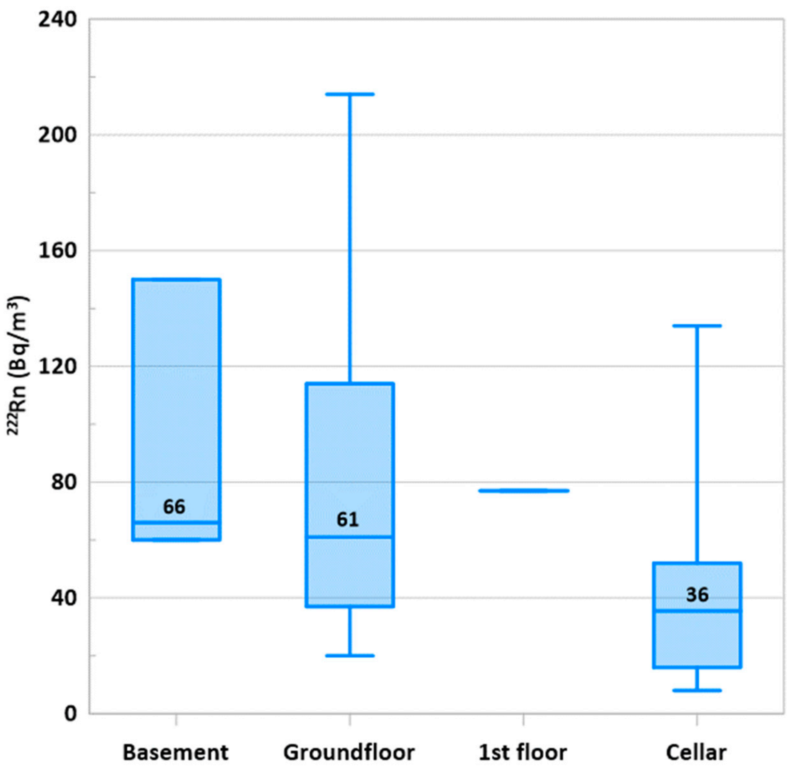

Figure 6. Comparison among indoor radon values from the four types of ambience in the monitored houses, presented as box plots. The box plots are composed of lower and upper quartiles (box edges), median (the horizontal line inside the box and relative value), and whiskers (defined by minimum and maximum values) that show the spread of the data.

3.3. Radon Continuous Monitoring

The location of the sites monitored for continuous indoor Rn is shown in Figure 1. Apart from site #1, located inside the headquarters of INGV and chosen as the background, the other sites were selected (i) based on the results from the screening survey; (ii) based on their proximity to known faults or old eruptive fissures on the flanks of Mt. Etna, and/or (iii) because they are home to patients with neurodegenerative diseases (mostly Multiple

Sclerosis, Amyotrophic Lateral Sclerosis, and Primary Brain Tumors like meningiomas and glioblastomas).

In one of the sites where the indoor Rn levels were found to be particularly high (namely, site #8), a fixed station for monitoring the concentration of radon both in the soil and in the air 1 m above the ground was installed in a garden about 10 m outside of the house. In this way, we wanted to study how radon diffuses from the ground surface into the atmosphere by monitoring the Rn concentration gradient in the air and how those results may correlate with indoor Rn concentrations measured inside the house.

Figure 7 shows the results of continuous indoor radon monitoring in the fifteen sites selected on Mt. Etna during the period from July 2021 to February 2024, whereas Table 4 shows some descriptive statistics on the values obtained at each site. Twelve out of the fifteen sites were chosen among those where indoor radon levels were previously measured using charcoal canisters. The monitoring periods were different among sites due to the unavailability of the site before or after the monitoring period. Furthermore, periods with missing data occurred because of power failures (i.e., the batteries have run out) and/or because of the saturation of the data logger memory of the monitoring instrument.

Table 4. Descriptive statistics on the indoor radon data from the 15 monitoring sensors located on Mt. Etna. All values are expressed in Bq/m^3.

Site	Number of Measurements	Min	Max	Mean	Standard Deviation	Median	Mode	Skewness
AER1	67,443	0	504	55	66	72	0	1.32
AER2	57,925	0	598	65	80	66	0	1.49
AER3	65,230	0	594	54	69	66	0	1.59
AER4	53,045	0	391	39	54	0	0	1.52
AER5	62,493	0	1461	138	157	66	0	1.65
AER6	42,395	0	2230	56	72	66	0	2.31
AER7	41,481	0	2656	294	300	199	66	1.82
AER8	73,484	0	1452	159	165	132	0	1.37
AER9	38,429	0	1146	52	73	0	0	1.88
AER10	46,539	0	5472	392	616	137	0	2.32
AER11	44,952	0	406	28	46	0	0	1.69
AER12	9988	0	835	112	105	70	70	1.05
AER13	26,591	0	2800	298	335	210	0	1.63
AER14	4486	0	1340	352	212	365	35	0.25
AER15	10,016	0	6048	3121	1407	3600	3744	−0.97

The table also shows that all of the maximum radon values were higher than the radon threshold (300 Bq/m^3) set for indoor radon exposure by the 2013/59 Euratom Directive and that the variability of the single datasets was often very high. Furthermore, all datasets, except that of AER15, were highly skewed towards the left, thus pointing to a log-normal distribution of the data; i.e., the largest majority of the data is represented by low values. Site AER15 is an exception because the largest majority of the values measured were stable at very high levels of radon concentration for a long period. The temporal patterns of the data shown in the plots of Figure 7 highlight that higher radon values were normally recorded during the winter period. This is the typical behavior of radon accumulation into houses, because during the cold winter months people tend to keep doors and windows closed, thus preventing efficient air circulation and, hence, radon dilution. Furthermore, heating in winter may cause the chimney effect, thus causing radon to enter from the basement of homes. Isolated spikes in the radon values (i.e., lasting only one measurement period) may have been caused by momentary electric problems of the sensors (for example, during the replacement of the battery) or due to the involuntary exposure of the sensor to direct light.

The main result of the radon continuous monitoring is that the largest majority of the monitored sites (14 out of 15) showed radon values that, even if slightly and for short periods, were higher than the radon exposure threshold. This finding underlines the need of a long-term monitoring—for at least several months—of indoor radon on Mt. Etna, because radon values may be subject to dramatic changes, even by orders of magnitude, in the different seasons of the year.

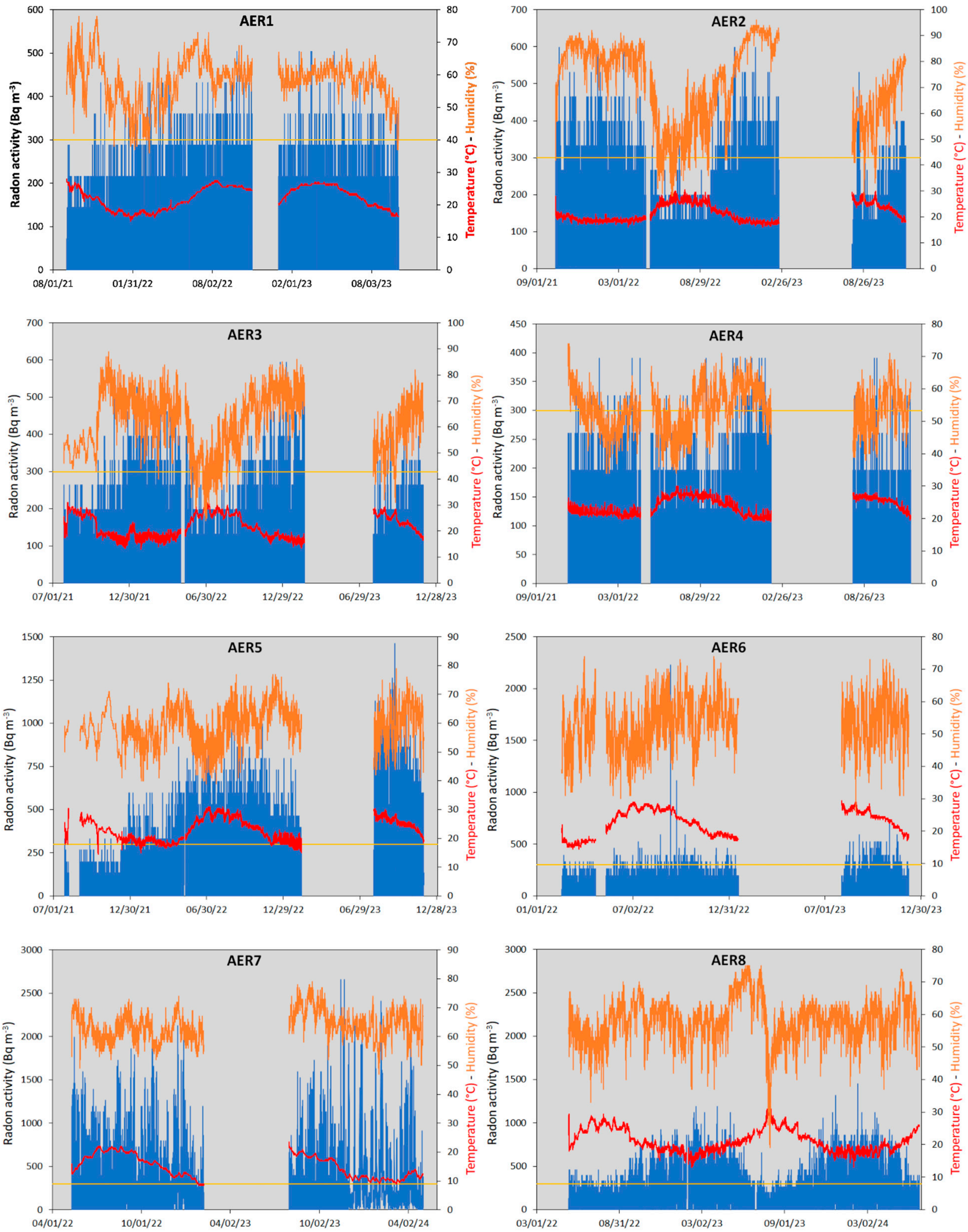

Figure 7. *Cont.*

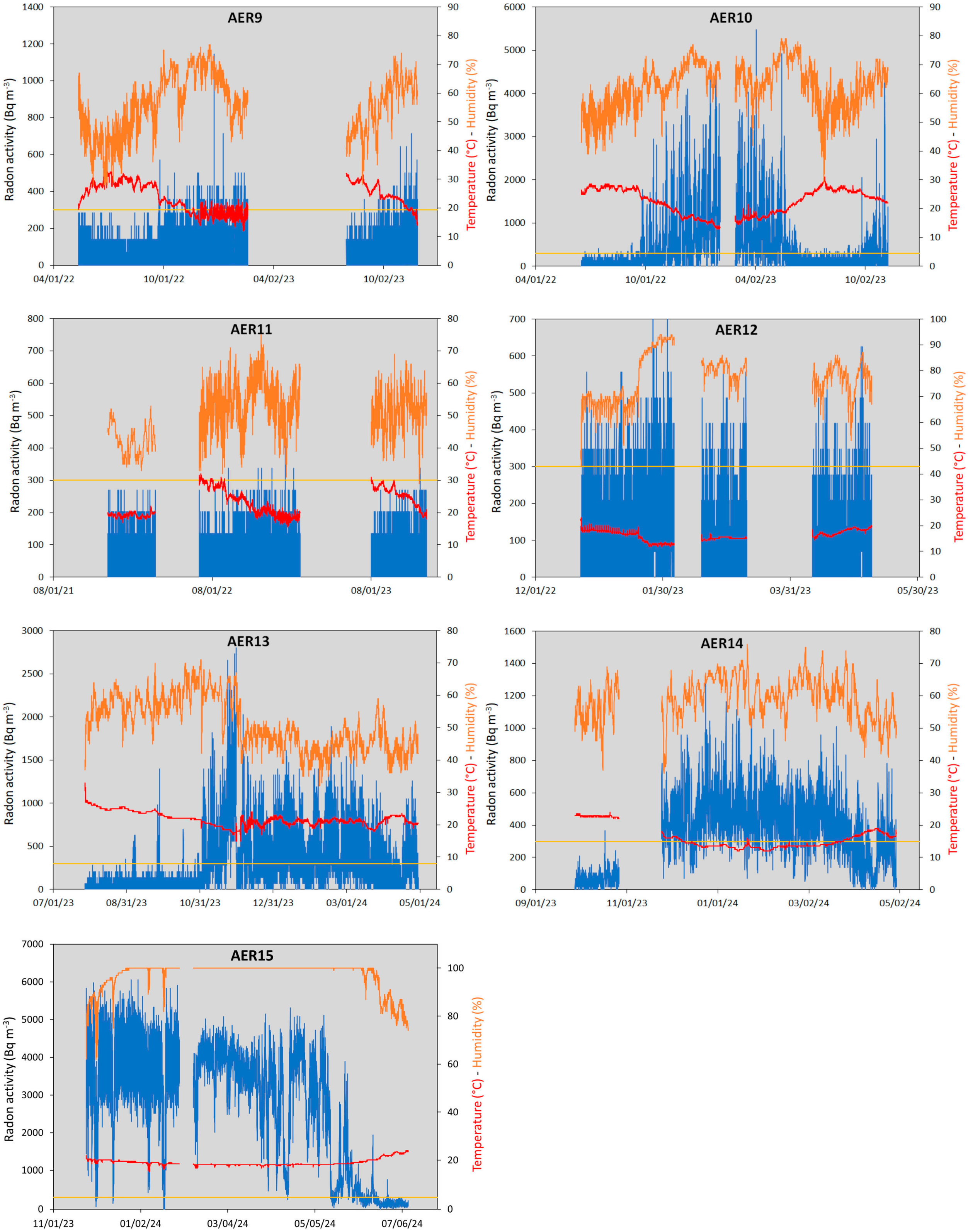

Figure 7. Results of the continuous monitoring of indoor radon in the 15 sites selected on Mt. Etna from 2021 to 2024. In all plots, blue curves indicate the radon activity (in Bq/m^3), orange curves the indoor air humidity (in %), red curves the indoor air temperature (in °C), and the yellow horizontal lines the radon threshold (300 Bq/m^3) admitted for indoor radon exposure by the 2013/59 Euratom Directive.

The site named AER15 is a very peculiar site, because of its nature and because the behavior of the monitored parameters is somewhat exceptional. The radon sensor was located inside the hypogeum of the main church of Trecastagni, where peculiar environmental conditions occur because of a strong emission of gas and steam from the deepest point of the basement of one of the underground rooms beneath the church. On the other hand, it should be noted that the church was built on top of an ancient pyroclastic cone [47]. In those rooms, during winter and spring, the ambient air showed an almost constant temperature of 19 °C, the air humidity was close to 100%, the ambient CO_2 concentration was about 1200 ppm vol (S.G., unpublished data), and the indoor radon activity was almost stable at around 3800 Bq/m^3 (Figure 7). Until May 2024, short periods with much lower values of all monitored parameters were due to the forced air ventilation from outside in order to dilute the gases and allow church staff access to the premises for cleaning and maintenance. During the warmer months, however, all parameters showed a marked decrease, in agreement with the general pattern observed at all monitoring stations. In particular, radon values dropped to very low values that remained almost constantly below 300 Bq/m^3 until the end of the monitoring period.

4. Discussion

The results of the present study confirm that radon emissions in a volcanic area occur not only from open craters or vents, but also from the soils along the volcano flanks, mostly along tectonic or volcano-tectonic structures [18,22,40]. Soil radon emissions in the study area of Pedara–Trecastagni clearly show their highest values both along a major tectonic fault line (Trecastagni fault) and along an ancient eruptive fissure that formed a large cinder cone called Mt. Troina, whose age has been set between 3930 ± 60 a and the eruption of 122 BC [47]. This confirms the results obtained by Bonforte et al. [22], which highlighted the presence of an anomalous increase in radon and CO_2 emissions from soil in correspondence with volcano-tectonic structures cropping out in the Pedara–Trecastagni area [47,48]. Furthermore, other in-soil radon anomalies, mostly regarding ^{222}Rn, are located further east inside the town of Trecastagni and they correspond with the highest indoor radon values found in homes of that town (i.e., AER13, AER14, and AER15). These anomalous sites are located on an ancient pyroclastic cone, on which the church of Trecastagni was built, that has been dated between 15,000 and 3930 ± 60 years [47]. This evidence strongly suggests that both the Mt. Troina cinder cone and the ancient Trecastagni pyroclastic cone are located on deeper and still active volcano-tectonic structures that are driving volcanic gases (including hot steam, CO_2, and radon) to the surface.

The cause–effect relationship between the presence of faults/fissures and higher radon emissions is clearly shown in Figure 8. In this figure, the long-term average values of indoor radon concentration measured in all our sites is plotted versus the distance between each site and the closest tectonic fault or the closest old eruptive fissure. In the figure are also shown, as blue circles, the average values obtained from a previous investigation focused only on long-term indoor radon monitoring, using similar digital monitors as those used in this study [41]. Our results further strengthen the model of radon dispersion in ambient air that was obtained in the previous work, as we observed a significant correlation between all of the averages available and the distances of monitoring sites from faults/fissures. The overall best-fit model for the data actually follows a negative power law: $y = 3058.6\ x^{-0.537}$, with $R^2 = 0.58$. This means that, in order to have average radon values within the maximum threshold of 300 Bq/m^3 recommended by the WHO handbook [32], homes should be located at least 300 m away from faults or eruptive fissures. Furthermore, in order to be exposed to indoor radon average values lower than the limit of 100 Bq/m^3 recommended as the attention threshold by the WHO [32], a reasonable safe distance from faults or eruptive fissures would be much higher, at least 1800 m.

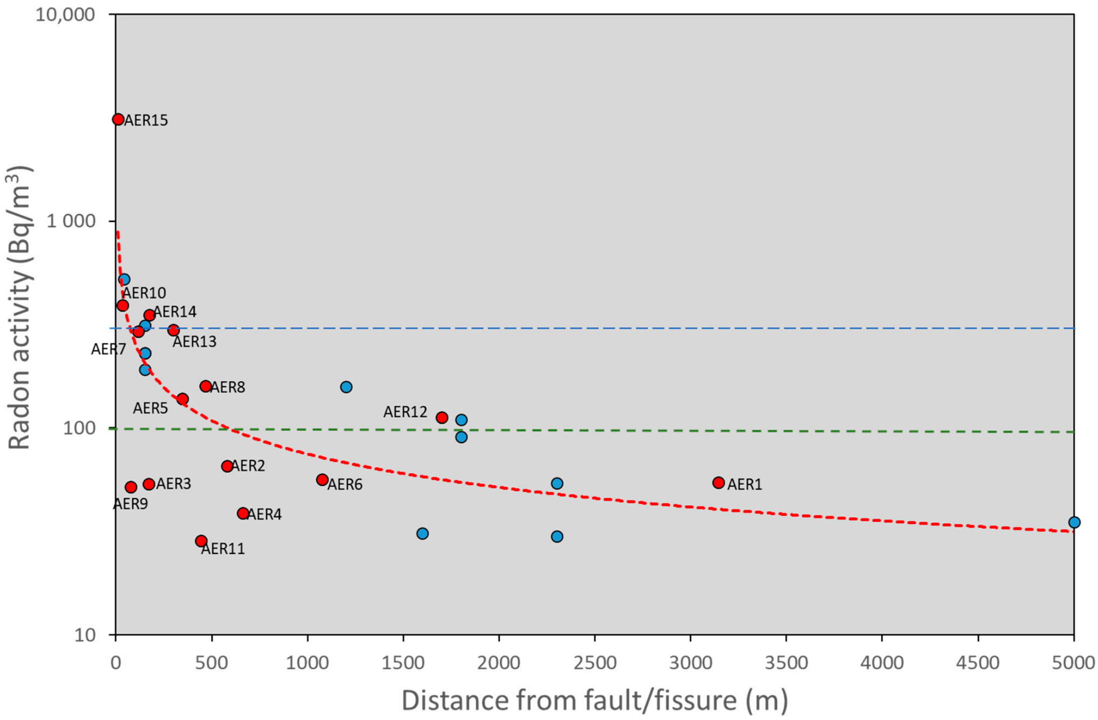

Figure 8. Diagram showing the correlation between long-term averages of indoor radon activity and distance of monitoring sites from known active faults or eruptive fissures. The red-filled circles represent our data, which have been labeled according to Table 2. The blue-filled circles show the data from [41]. The blue dashed line represents the maximum threshold (300 Bq/m^3) recommended by the World Health Organization (WHO) handbook [32]. The green dashed line indicates the limit of 100 Bq/m^3 recommended by the WHO as an attention threshold. The dotted red line represents the best-fit model for all of the data, which follows a power law (y = 3058.6x$^{-0.537}$, with R^2 = 0.58).

The data from the continuous monitoring station located outside site AER8 are shown in Figure 9. As expected, in-soil radon values were higher than those measured at a 1 m height, and a general mild temporal correlation can be observed between the two sets of data (e.g., both display higher values during the winter and lower values during the summer, and some of the negative or positive spikes overlap). On average, the ratio between air radon values at 1 m and ground radon values was about 0.47. This means that a significant part of the radon emitted through the soil surface around the house was able to migrate to the atmosphere. By comparing the cumulated hourly activity of radon measured indoors and that measured with the outdoor station during the same period (from 26 June 2023 to 30 April 2024), both in the ground and in the air at 1 m, we found that the best correlation was between the indoor hourly data and ground values (R^2 = 0.37). Although not so strong from a statistical point of view, the observed correlation points to a mechanism of indoor radon accumulation closely related both to the amount of radon in soil and to the efficiency of radon transfer from the ground to indoor environments.

In order to more accurately evaluate the potential influence of indoor radon accumulation on human health in the specific cases examined in this investigation, the annual mean effective dose H (in mSv y^{-1}) at each location was estimated, in accordance with the methodology outlined by UNSCEAR [23,24]. To achieve this, the following approach was employed:

$$H = C \times E \times F \times T \times D \quad (2)$$

In this model, C represents the average radon concentration measured at each location over the specified monitoring period. E is an equilibrium factor, which, in this case, is set at 0.4. F is the occupancy factor, calculated as the percentage of time spent in each site, depending on the room type. In this model, the occupancy factor for sites AER1 and AER15 is set at 0.20, given the infrequent occupancy of the room, and at 0.75 for the other sites. T is the number of hours in a year, or 8760 h. D is a dose conversion factor, set at 9.0×10^{-6} mSv/Bq h m^{-3}. The resulting dose values are presented in Table 5. The values ranged from 0.35 to 19.69 mSv y^{-1}, with a mean value of 4.55 mSv y^{-1}. With the exception of site AER15, all other sites were characterized by doses within the global range of values for the internal exposure to natural sources of radiation (1–10 mSv y^{-1}, as outlined in [24]). The mean value derived from the present investigation, however, is considerably higher than the estimated worldwide annual effective dose per person (2.40 mSv y^{-1} [24]). Notably, some of the highest doses were observed in the houses of individuals diagnosed with neurodegenerative disorders.

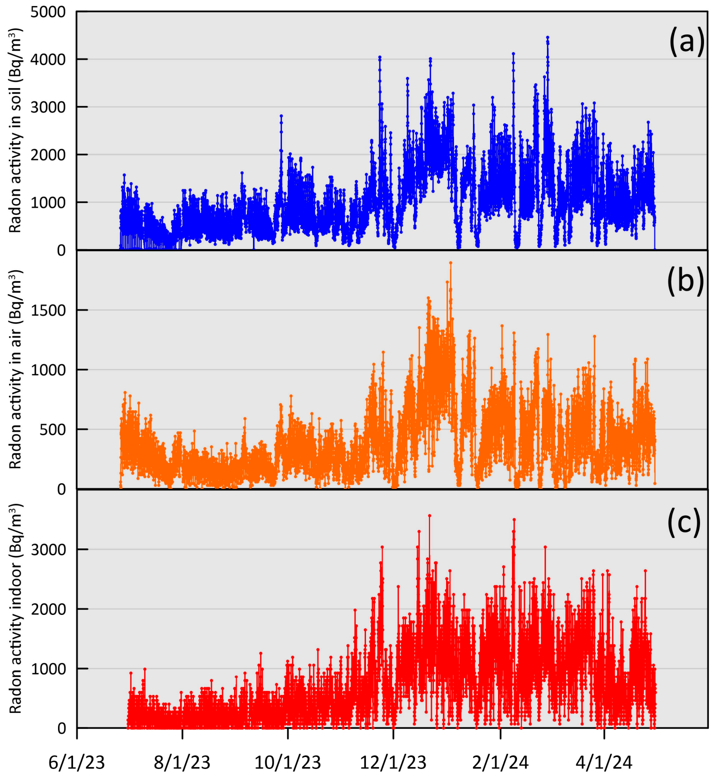

Figure 9. Radon data from the continuous monitoring station located outside site AER8, confronted with indoor radon values at the same site measured during the same period: (**a**) radon activity values measured in the ground at 50 cm depth; (**b**) radon activity values measured in the air at a height of 1m above the ground; and (**c**) radon activity values measured indoor (values measured every 15 min were integrated over 1 h periods in order to make them comparable with the continuous radon data).

Table 5. Annual mean effective dose H at each location of continuous indoor monitoring sensors, estimated following the procedure indicated by UNSCEAR [23,24].

Site	Dose (mSv y^{-1})
AER1	0.35
AER2	1.55
AER3	1.27
AER4	0.92
AER5	3.27
AER6	1.33
AER7	6.95
AER8	3.77
AER9	1.22
AER10	9.27
AER11	0.67
AER12	2.66
AER13	7.04
AER14	8.32
AER15	19.69

5. Conclusions

The combined soil radon-gas measurements in air and in soil carried out in the S and E flanks of Mt. Etna from 2021 to 2024 confirmed and better assessed the widespread and significant diffuse emission of this gas on this volcano and expanded our knowledge on the process of radon emission and accumulation in houses. Furthermore, our results highlighted the spatial link between faults and strong radon gas emissions.

Clear linear anomalies of ^{222}Rn and ^{220}Rn were found close to known active faults that, because of their higher porosity and permeability in comparison with the surrounding soil, act as a preferential way of gas migration towards the surface.

Discrete indoor radon measurements in homes located in the studied areas revealed that basements have the highest radon values, although they remain below the radon threshold (300 Bq/m^3) allowed for indoor radon exposure by the 2013/59 Euratom Directive. On the other hand, the continuous monitoring of indoor radon activity carried out over periods of some years allowed for more detailed information on the temporal changes of this parameter, thus showing that, during the winter months, the indoor radon concentrations were always much higher than those recorded during the summer months and they were often much higher than the indoor radon threshold of 300 Bq/m^3 set by the 2013/59 Euratom Directive.

This behavior confirms what was already observed in previous similar investigations carried out in other areas of Mt. Etna [41], thus strengthening the need for an accurate site-by-site continuous monitoring of indoor radon levels and a thorough evaluation of the mechanisms of radon transfer from the soil to the houses. The correlation between high radon doses indoors and neurodegenerative diseases suggests a possible cause–effect relationship that needs to be investigated further.

In conclusion, our results shed some more light on the way radon gas is released in a volcanic environment such as that of Mt. Etna and how it is transferred into the atmosphere and into houses. It is acknowledged that the data sample obtained and analyzed is relatively limited in size. Nevertheless, the outcomes yielded are definitive and warrant immediate dissemination to the residents of Etna, particularly those situated in proximity to tectonic or volcano-tectonic faults, in order to provide comprehensive information regarding the potential hazards associated with prolonged exposure to indoor radon. Additionally, the findings should be employed to encourage the implementation of remediation strategies.

Author Contributions: Conceptualization, M.N. and S.G.; methodology, N.V., S.G., G.G. and M.N.; validation, N.V., S.G., G.G., A.G. and M.N.; formal analysis, N.V., S.G. and G.G.; investigation, N.V., S.G., G.G. and A.G.; data curation, N.V., S.G. and G.G.; writing—original draft preparation, N.V., S.G. and M.N.; writing—review and editing, N.V., S.G. and M.N.; supervision, M.N.; project administration, N.V. and S.G.; funding acquisition, S.G. All authors have read and agreed to the published version of the manuscript.

Funding: This research was funded in part by the Ministry of University and Research of Italy, project "INGV Pianeta Dinamico, Tema 8-HEAVEN-2021", and in part by the Istituto Nazionale di Geofisica e Vulcanologia, "Bando di Ricerca Libera 2019-project IRHAFaults".

Institutional Review Board Statement: Not applicable.

Informed Consent Statement: Informed consent was obtained from all subjects involved in the study.

Data Availability Statement: The raw data from indoor radon monitoring will be made available by the authors upon request.

Acknowledgments: The authors wish to thank all the people that gave them permission to set up the radon monitors in their homes, and to perform radon measurements both indoors and in soil inside their private properties.

Conflicts of Interest: The authors declare no conflicts of interest.

References

1. Conner, C.; Hill, B.; LaFemina, P.; Navarro, M.; Conway, M. Soil 222Rn pulse during the initial phase of the June-August 1995 eruption of Cerro Negro, Nicaragua. *J. Volcanol. Geotherm. Res.* **1996**, *73*, 119–127. [CrossRef]
2. Etiope, G.; Martinelli, G. Migration of carrier and trace gases in the geosphere: An overview. *Phys. Earth Planet. Int.* **2002**, *129*, 185–204. [CrossRef]
3. Immè, G.; Morelli, D. Radon survey in active volcanoes. In *Handbook of Radon: Properties, Applications and Health*; Nova Science Publishers: Hauppauge, NY, USA, 2012; pp. 405–416.
4. Cigolini, C.; Laiolo, M.; Ulivieri, G.; Coppola, D.; Ripepe, M. Radon mapping, automatic measurements and extremely high ^{222}Rn emissions during the 2002–2007 eruptive scenarios at Stromboli volcano. *J. Volcanol. Geotherm. Res.* **2013**, *256*, 49–65. [CrossRef]
5. Cigolini, C.; Laiolo, M.; Coppola, D.; Ulivieri, G. Preliminary radon measurements at Villarrica volcano, Chile. *J. South Am. Earth Sci.* **2013**, *46*, 1–8. [CrossRef]
6. Ichedef, M.; Giammanco, S.; Neri, M.; Catalano, R.; Immé, G.; Morelli, D.; Muré, F.; Giudice, N. In soil radon anomalies and volcanic activity on Mt. Etna (Italy). *J. Environ. Radioact.* **2020**, *218*, 106267. [CrossRef]
7. Morelli, D.; Di Martino, S.; Immè, G.; La Delfa, S.; Lo Nigro, S.; Patanè, G. Evidence of soil radon as tracer of magma uprising in Mt. Etna. *Radiat. Meas.* **2006**, *41*, 721–725. [CrossRef]
8. Pinault, J.L.; Baubron, J.C. Signal processing of soil gas radon, atmospheric pressure, moisture, and soil temperature data: A new approach for radon concentration modeling. *J. Geophys. Res. Solid Earth* **1996**, *101*, 3157–3171. [CrossRef]
9. Falsaperla, S.; Neri, M.; Di Grazia, G.; Langer, H.; Spampinato, S. What happens to in-soil radon activity during a long-lasting eruption? Insights from Etna by multidisciplinary data analysis. *Geochem. Geophys. Geosystems* **2017**, *18*, 2162–2176. [CrossRef]
10. King, C.Y. Radon emanation on San Andreas Fault. *Nature* **1978**, *271*, 516–519. [CrossRef]
11. King, C.Y.; King, B.S.; Evans, W.C. Spatial radon anomalies on active faults in California. *Appl. Geochem.* **1996**, *11*, 497–510. [CrossRef]
12. Toutain, J.P.; Baubron, J.C. Gas geochemistry and seismotectonics: A review. *Tectonophysics* **1999**, *304*, 1–27. [CrossRef]
13. Woith, H. Radon earthquake precursor: A short review. *Eur. Phys. J. Spec. Top.* **2015**, *224*, 611–627. [CrossRef]
14. Baubron, J.-C.; Rigo, A.; Toutain, J.-P. Soil gas profiles as a tool to characterise active tectonic areas: The Jaut Pass example (Pyrenees, France). *Earth Planet. Sci. Lett.* **2002**, *196*, 69–81. [CrossRef]
15. Giammanco, S.; Immè, G.; Mangano, G.; Morelli, D.; Neri, M. Comparison between different methodologies for detecting Radon in soil along an active fault: The case of the Pernicana fault system, Mt. Etna. *Appl. Radiat. Isot.* **2009**, *67*, 178–185. [CrossRef] [PubMed]
16. Wang, X.; Li, Y.; Du, J.; Zhou, X. Correlations between radon in soil gas and the activity of seismogenic faults in the Tangshan area, North China. *Radiat. Meas.* **2014**, *60*, 8–14. [CrossRef]
17. Yasuoka, Y.; Kawada, Y.; Nagahama, H.; Omori, Y.; Ishikawa, T.; Tokonami, S.; Shinogi, M. Preseismic changes in atmospheric radon concentration and crustal strain. *Phys. Chem. Earth* **2009**, *34*, 431–434. [CrossRef]
18. Neri, M.; Ferrera, E.; Giammanco, S.; Currenti, G.; Cirrincione, R.; Patanè, G.; Zanon, V. Soil radon measurements as a potential tracer of tectonic and volcanic activity. *Sci. Rep.* **2016**, *6*, 24581. [CrossRef]
19. Siniscalchi, A.; Tripaldi, S.; Neri, M.; Giammanco, S.; Piscitelli, S.; Balasco, M.; Behncke, B.; Magrì, C.; Naudet, V.; Rizzo, E. Insights into fluid circulation across the Pernicana Fault (Mt. Etna, Italy) and implications for flank instability. *J. Volcanol. Geotherm. Res.* **2010**, *193*, 137–142. [CrossRef]
20. Vizzini, F.; Brai, M. In-soil radon anomalies as precursors of earthquakes: A case study in the SE slope of Mt. Etna in a period of quite stable weather conditions. *J. Environ. Radioact.* **2012**, *113*, 131–141. [CrossRef]
21. Falsaperla, S.; Behncke, B.; Langer, H.; Neri, M.; Salerno, G.; Giammanco, S.; Pecora, E.; Biale, E. "Failed" eruptions revealed by the study of gas emission and volcanic tremor data at Mt. Etna, Italy. *Int. J. Earth Sci. (Geol. Rundsch.)* **2014**, *103*, 297–313. [CrossRef]
22. Bonforte, A.; Federico, C.; Giammanco, S.; Guglielmino, F.; Liuzzo, M.; Neri, M. Soil gases and SAR data reveal hidden faults on the sliding flank of Mt. Etna (Italy). *J. Volcanol. Geotherm. Res.* **2013**, *251*, 27–40. [CrossRef]
23. UNSCEAR. *Ionizing Radiation: Sources and Biological Effects*; United Nations Scientific Committee on the Effects of Atomic Radiation; United Nations Publication: New York, NY, USA, 1982; pp. 1–773.
24. UNSCEAR. *Sources and Effects of Ionizing Radiation*; United Nations Scientific Committee on the Effects of Atomic Radiation; United Nations Publication: New York, NY, USA, 2000; pp. 1–654.
25. Muirhead, C.R. Radon risks. *Lancet* **1994**, *344*, 143–144. [CrossRef] [PubMed]
26. Groves-Kirkby, C.J.; Denman, A.R.; Phillips, P.S.; Crockett, R.G.M.; Sinclair, J.M. Comparison of seasonal variability in European domestic radon measurements. *Nat. Hazards Earth Syst. Sci.* **2010**, *10*, 565–569. [CrossRef]
27. Darby, S.; Hill, D.; Auvinen, A.; Barros-Dios, J.M.; Baysson, H.; Bochicchio, F.; Deo, H.; Falk, R.; Forastiere, F.; Hakama, M.; et al. Radon in homes and risk of lung cancer: Collaborative analysis of individual data from 13 European case-control studies. *Br. Med. J.* **2005**, *330*, 223–227. [CrossRef]
28. Darby, S.; Hill, D.; Deo, H.; Auvinen, A.; Barros-Dios, J.M.; Baysson, H.; Bochicchio, F.; Falk, R.; Farchi, S.; Figueiras, A.; et al. Residential radon and lung cancer: Detailed results of a collaborative analysis of individual data on 7148 subjects with lung cancer and 14208 subjects without lung cancer from 13 epidemiologic studies in Europe. *Scand. J. Work Environ. Health* **2006**, *32* (Suppl. S1), 1–83.

29. Gray, A.; Read, S.; McGale, P.; Darby, S. Lung cancer deaths from indoor radon and the cost effectiveness and potential of policies to reduce them. *Br. Med. J.* **2009**, *338*, a3110. [CrossRef]
30. Henyoh, A.M.S.; Laurent, O.; Mandin, C.; Clero, E. Radon exposure and potential health effects other than lung cancer: A systematic review and meta-analysis. *Front. Public. Health* **2024**, *12*, 1439355. [CrossRef]
31. Tong, J.; Qin, L.; Cao, Y.; Li, J.; Zhang, J.; Nie, J.; An, Y. Environmental radon exposure and childhood leukemia. *J. Toxicol. Environ. Health B Crit. Rev.* **2012**, *15*, 332–347. [CrossRef]
32. WHO. *WHO Handbook on Indoor Radon: A Public Health*; World Health Organization: Geneva, Switzerland, 2009; pp. 1–95.
33. Immè, G.; La Delfa, S.; Lo Nigro, S.; Morelli, D.; Patanè, G. Gas radon emission related to geodynamic activity on. Mt. Etna. *Ann. Geophys.* **2005**, *48*, 65–71. [CrossRef]
34. La Delfa, S.; Immè, G.; Lo Nigro, S.; Morelli, D.; Patanè, G.; Vizzini, F. Radon measurements in the SE and NE flank of Mt. Etna (Italy). *Radiat. Meas.* **2007**, *42*, 1404–1408. [CrossRef]
35. Immè, G.; La Delfa, S.; Lo Nigro, S.; Morelli, D.; Patanè, G. Soil radon concentration and volcanic activity of Mt. Etna before and after the 2002 eruption. *Radiat. Meas.* **2006**, *41*, 241–245. [CrossRef]
36. Brogna, A.; La Delfa, S.; La Monaca, V.; Lo Nigro, S.; Morelli, D.; Patane', G.; Tringali, G. Measurements of indoor radon concentration on the south-eastern flank of Mount Etna volcano (Southern Italy). *J. Volcanol. Geotherm. Res.* **2007**, *165*, 71–75. [CrossRef]
37. La Delfa, S.; Agostino, I.; Morelli, D.; Patanè, G. Soil radon concentration and effective stress variation at Mt. Etna (Sicily) in the period January 2003–April 2005. *Radiat. Meas.* **2008**, *43*, 1299–1304. [CrossRef]
38. La Delfa, S.; Vizzini, F.; Patanè, G. Radon migration into different building types at medium and low south-eastern flank of Mt Etna (Sicily): Connection with the volcanic activity. *Environ. Earth Sci.* **2012**, *66*, 923–931. [CrossRef]
39. Neri, M.; Giammanco, S.; Ferrera, E.; Patanè, G.; Zanon, V. Spatial distribution of soil radon as a tool to recognize active faulting on an active volcano: The example of Mt. Etna (Italy). *J. Environ. Radioact.* **2011**, *102*, 863–870. [CrossRef]
40. Giammanco, S.; Bonfanti, P.; Neri, M. Radon on Mt. Etna (Italy): A useful tracer of geodynamic processes and a potential health hazard to populations. *Front. Earth Sci.* **2023**, *11*, 1176051. [CrossRef]
41. Neri, M.; Giammanco, S.; Leonardi, A. Preliminary Indoor Radon Measurements Near Faults Crossing Urban Areas of Mt. Etna Volcano (Italy). *Front. Public Health* **2019**, *7*, 105. [CrossRef]
42. Zhang, B.; Liu, H.; Crawford, J.H.; Chen, G.; Fairlie, T.D.; Chambers, S.; Kang, C.H.; Williams, A.G.; Zhang, K.; Considine, D.B.; et al. Simulation of radon-222 with the GEOS-chem global model: Emissions, seasonality, and convective transport. *Atmos. Chem. Phys.* **2021**, *21*, 1861–1887. [CrossRef]
43. Galli, G.; Cannelli, V.; Nardi, A.; Piersanti, A. Implementing soil radon detectors for long term continuous monitoring. *Appl. Radiat. Isot.* **2019**, *153*, 108813. [CrossRef]
44. Galli, G.; Guadoni, C.; Mancini, C. Radon grab sampling in water by means of radon transfer in activated charcoal collector. *Il Nuovo C.* **1999**, *22*, 583–588.
45. De Luca, A.; Mancini, C. The measurement system for ^{222}Rn monitoring with charcoal adsorption collectors. *Health Phys.* **1991**, *61*, 543–546. [CrossRef] [PubMed]
46. Sinclair, A.J. A fundamental approach to threshold estimation in exploration geochemistry: Probability plots revisited. *J. Geochem. Explor.* **1991**, *41*, 1–22. [CrossRef]
47. Branca, S.; Coltelli, M.; Groppelli, G. Geological evolution of a complex basaltic stratovolcano: Mount Etna. Italy. *Ital. J. Geosci.* **2011**, *130*, 306–317. [CrossRef]
48. Urlaub, M.; Petersen, F.; Gross, F.; Bonforte, A.; Puglisi, G.; Guglielmino, F. Gravitational collapse of Mount Etna's southeastern flank. *Sci. Adv.* **2018**, *4*, eaat9700. [CrossRef]